Journal of Industrial Microbiology & Biotechnology (2001) 26, 43–52

www.nature.com/jim

Use of ^{1}H NMR to study transport processes in porous biosystems

HV As and P Lens

Wageningen NMR Centre and Laboratory of Molecular Physics, Wageningen University, Dreijenlaan 3, 6703 HA, Wageningen, Netherlands

The operation of bioreactors and the metabolism of microorganisms in biofilms or soil/sediment systems are strongly dictated by the transport processes therein. Nuclear magnetic resonance (NMR) spectroscopy or magnetic resonance imaging (MRI) allow nondestructive and noninvasive quantification and visualisation (in case of MRI) of both static and dynamic water transport phenomena. Flow, mass transfer and transport processes can be measured by mapping the (proton) displacement in a defined time interval directly in a so-called pulsed field gradient (PFG) experiment. Other methods follow the local intensity in time-controlled sequential images of water or labelled molecules, or map the effect of contrast agents. Combining transport measurements with relaxation-time information allows the discrimination of transport processes in different environments or of different fluids, even within a single picture element in an image of the porous biosystem under study. By proper choice of the applied NMR method, a time window ranging from milliseconds to weeks (or longer) can be covered. In this paper, we present an overview of the principles of NMR and MRI techniques to visualise and unravel complex, heterogeneous transport processes in porous biological systems. Applications and limitations will be discussed, based on results obtained in (model) biofilms, bioreactors, microbial mats and sediments. *Journal of Industrial Microbiology & Biotechnology* (2001) **26,** 43–52.

Keywords: transport processes; magnetic resonance microscopy; diffusion; dispersive flow; bioreactors; biofilms; sludge; porous media; soils

Introduction

Porous biosystems are ubiquitous in both natural and man-made ecosystems, i.e., sludges or biofilms in bioreactors, soils or sediments. Transport processes in these biological microporous systems depend strongly on the local amount of water, the interaction of the transport medium with the particles, and the pore dimensions/geometry (e.g., the porosity and tortuosity). Different types of transport processes, e.g., diffusion, perfusion and convection, can be distinguished in porous biosystems (Figure 1).

Substrate conversion rates in porous biosystems are strongly dictated by the transport processes. Most bioreactor, biofilm and soil/sediment reactions are diffusion limited, and the concentration gradients that develop within these systems are determined by molecular diffusivity and convection. To determine the rate-limiting transport process and to optimise it, there is a strong interest in the direct and noninvasive measurement of transport processes in these complex biosystems [2,55].

A range of transport measurement methods are presently available to determine the transport processes within porous biosystems, including laser Doppler anemometry and X-ray transmission or diffraction tomography [7], microsensors [9,25], scanning confocal laser microscopy and fluorescence recovery after photobleaching [9,39], microwave and ultrasonic tomography [7]. The major attraction of NMR over these methods is that it is noninvasive, so that no direct contact with the fluid is necessary [6] and it uses naturally present labels such as ^{1}H, ^{13}C, ^{15}N and ^{31}P. Hence, it is well suited for studies of liquids that need to be isolated, such as those having extreme temperature, chemical reactivity or which are abrasive. NMR does not use ionising radiation, in contrast to X-ray scattering flow methods. Another special property of NMR is that flow can be detected in any direction within the sample, in contrast to X-ray, optical and ultrasound scattering flow methods that only measure a net flow between the emitter and the detector.

NMR measurements allow the combined measurement of the anatomy and spin (^{1}H) density of a sample, simultaneously with the transport processes. These parameters can be only partly studied by other methods for transport studies such as tracer studies, breakthrough curves or by computer simulations based on 3D pore-geometry information from, e.g., X-ray computer tomography (e.g., Ref. [16]). The development of NMR imaging (MRI) has added a new aspect to NMR, namely image formation, resulting in the spatially resolved measurement of all information available with NMR in any selected part (volume, slice, etc.) of the system under observation. Thus, MRI provides a direct approach to the relation between the internal structure, local water (^{1}H) density and fluid (^{1}H of water or an organic compound) transport in a porous biosystem [14,63].

In this paper, the reader is first introduced to NMR parameters that can be used to describe transport processes, as well as to the measurement methods to determine these parameters. Then, three different approaches are presented to visualise and unravel complex, heterogeneous transport processes in porous biosystems. Their advantages and limitations will be discussed in relation to the time window over which transport processes can be measured and to the NMR properties of the porous biosystems.

NMR methods to study porous systems

A large number of nuclei, e.g., ^{1}H, ^{13}C, ^{19}F, ^{23}Na and ^{31}P, possess the property of *spin* [5]. NMR is a spectroscopic method based on the interaction between a radio frequency (rf) magnetic field and

Correspondence: Dr H Van As, Wageningen NMR Centre and Laboratory of Molecular Physics, Wageningen University, Dreijenlaan 3, 6703 HA Wageningen, Netherlands
Received 20 April 2000; accepted 14 August 2000

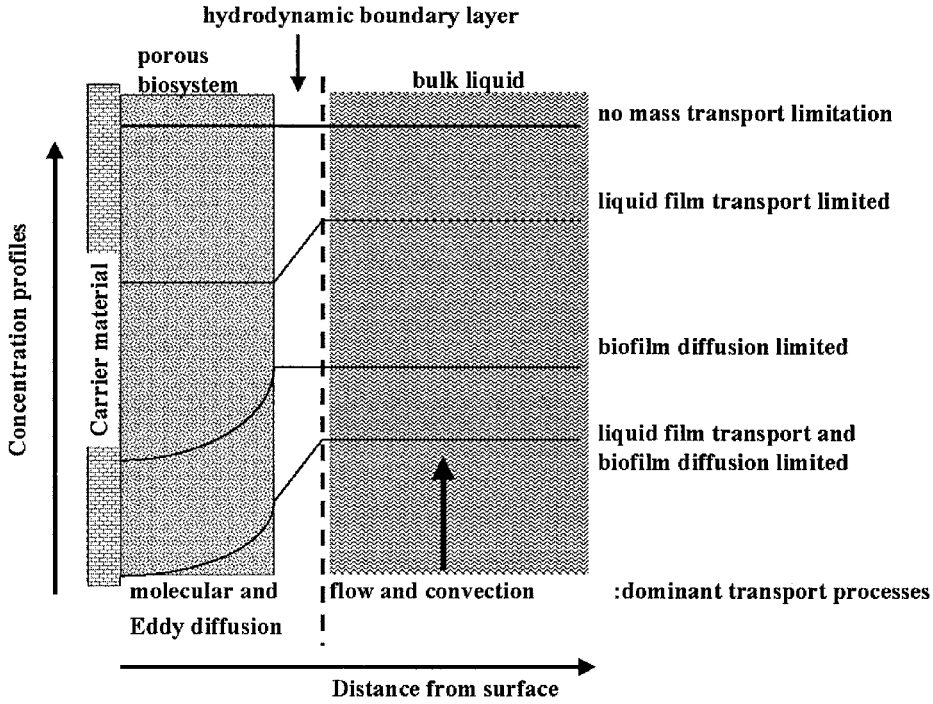

Figure 1 Schematic representation of substrate concentration profiles in and around a biofilm containing microorganism, for different transport conditions. The thickness of the hydrodynamic boundary layer will depend on the velocity and profile of the bulk liquid and on the roughness of the biofilm surface. The concentration profile in the biofilm is also dependent on the substrate conversion rate in this film.

the magnetic moments of these *spins* of samples placed in a magnetic field. The advantage is that the method is noninvasive, selective and transparent for porous biosystems. Its disadvantage is its inherent insensitivity. Of the NMR-measurable nuclei available in porous biosystems in natural abundance, ^{1}H is the most sensitive and has by far the highest concentration. Here we focus on ^{1}H NMR of water molecules in biosystems. More detailed descriptions of the basics of NMR and MRI can be found elsewhere [5,30].

NMR parameters

Excitation of spins by an rf pulse disturbs the equilibrium in the nuclear spin system. A time-dependent rf signal is induced in the NMR measuring probe by this nuclear spin system as it returns to equilibrium. These NMR signals are characterised by a number of different parameters. The amplitude A_0 of the NMR signal directly after excitation (time zero) is a direct measure for the amount of nuclei under observation in the NMR rf coil. If the volume is known A_0 directly relates to the density of nuclei under observation.

Two relaxation-time constants describe the rate and manner at which the nuclear spin system returns to equilibrium after excitation. One time constant, the spin–lattice relaxation time T_1, describes the return to the equilibrium state in the direction of the magnetic field. The second time constant, the spin–spin relaxation time T_2, characterises the return in the plane perpendicular to the applied magnetic field. Both relaxation times depend on the physical environment (pore size and geometry, adsorbing walls, packing density). Also the chemical composition of the liquid determines both relaxation times. Especially the presence of paramagnetic ions (e.g., Fe, Mn and Gd) drastically changes the T_1 and T_2 of water that is in contact with these ions, as these ions offer a very efficient relaxation pathway. Consequently, paramagnetic ions are applied as contrast or masking agents.

Magnetic resonance imaging (MRI)

In high-resolution NMR spectroscopy, a very homogeneous magnet is used to reduce line broadening effects, and the NMR signals are monitored for the whole sample. However, in magnetic resonance imaging (MRI), the resulting signal is recorded for a sample subdivided in a number of picture (pixels) or volume (voxels) elements by the use of strong magnetic field gradients applied to the sample. For sensitivity reasons, MRI is only practically feasible for studying highly abundant nuclei, e.g., ^{1}H, ^{23}Na or ^{31}P.

The frequency of the time-dependent rf signal given off by the nuclear spin system as it returns to equilibrium after being excited strongly depends on the magnetic field strength felt by the spins. When a well-defined linear magnetic field gradient is created, spins at different positions along this gradient give off rf signals with different frequencies. Consequently, each frequency is characteristic for a particular position. This is the basis for NMR imaging.

For the generation of NMR images, the NMR signal after being created has to be labelled for the respective positions by the use of magnetic field gradients. Position labelling by magnetic field gradients can be performed in a variety of ways (see e.g., Ref. [5]). Depending on the actual sequence used, the position-labelling process will take some time. In the most frequently used, so-called 2D Fourier transformed (FT) spin–echo (SE) sequence (2D-SE), acquisition of the signal occurs at a certain time TE (echo time) after the excitation of the spin system. During that time, the signal will decay according to the T_2 relaxation process:

$$A(\mathrm{TE}) = A_0 \exp(-\mathrm{TE}/T_2) \qquad (1)$$

The contrast or signal intensity in single SE images therefore strongly depends on TE. To obtain a full two-dimensional image of $N \times N$ picture elements, the sequence has to be repeated N times. If

the repetition time TR is long enough, the spin system has restored equilibrium along the magnetic field direction: TR > 3 T_1. If not, the signal amplitude does not uniquely represent the spin density in each pixel, but depends on a combination of the spin density and the relaxation time T_1. As a result, NMR image intensity usually depends on a combination of these parameters, reflecting spin density, T_1, T_2 and diffusion behaviour. By use of multiple echo image sequences single-parameter images of A_0, T_1 or T_2 can be constructed [5,11,13].

Self diffusion and flow measurements

Although effects of flow and motion on the NMR signal have been known for a long time, NMR has not been used very much for flow and (restricted) diffusion measurements in porous biosystems until recently. NMR is quite capable of discriminating proton spins of flowing and stationary water on the basis of the physical properties of flow [5,52,48,59]. The frequency of the signal given off by stationary spins will be constant in time, even in the presence of magnetic field gradients. However, when spins move from one position to another (diffusion, flow) in the presence of a magnetic field gradient, the frequency of these spins will change in time because of this displacement.

Diffusion and random dispersion do not result in a net displacement for the spin ensemble, and therefore do not result in a net frequency change, but in a broadening of the frequency bandwidth contributing to the signal. This results in a decrease in the signal amplitude. In contrast, net flow results in a frequency shift of the NMR signal originating from those moving spins, and becomes manifest as a phase shift of the NMR signal, because the NMR signal is detected with respect to a fixed reference frequency. This principle, applied in pulsed field gradient (PFG) NMR, allows one to discriminate and measure flow, dispersion and diffusion. PFG NMR flow methods have been described in detail by Caprihan and Fukushima [6], whereas PFG NMR techniques to determine self-diffusion coefficients are presented by Stilbs [56] and Le Bihan [28].

NMR parameters to characterise the porous biosystem

The amplitude and the relaxation times T_1 and T_2 are the most commonly applied NMR parameters to characterise porous biosystems.

In aqueous solutions, the amplitude of the ^{1}H NMR signal of water protons is a direct measure of the amount of water present in the sample. Thus, ^{1}H NMR can be used to determine the hydration state of solid wastes or sludges as a function of the drying process [27,47]. Additional information can be obtained about the water status of solid wastes when ^{1}H NMR amplitude measurements are performed spatially resolved (imaging) or combined with relaxation time or diffusion measurements (see below). However, some care must be taken to directly relate the amplitude information to the total amount of water in the system. Figure 2 illustrates the decay curve in a T_2 measurement from pollen grains. This figure clearly illustrates the multiexponential behaviour of the decay: a fast initial decay of part of the magnetisation (protons of the solid fraction and protons of "bound" water), whereas other parts decay more slowly (more freely water). In SE imaging and PFG measurements the first echo is detected at TE (cf. Equation 1), which is typically in the order of a few milliseconds or more. This can result in loss of part of the signal of the water fractions with short T_2 values, which are therefore not observed in these measurements.

The correlation between the value of the relaxation times T_1 and T_2 and pore dimensions in water-saturated porous media has been well investigated [22,24]. The relaxation times T_1 and T_2 strongly

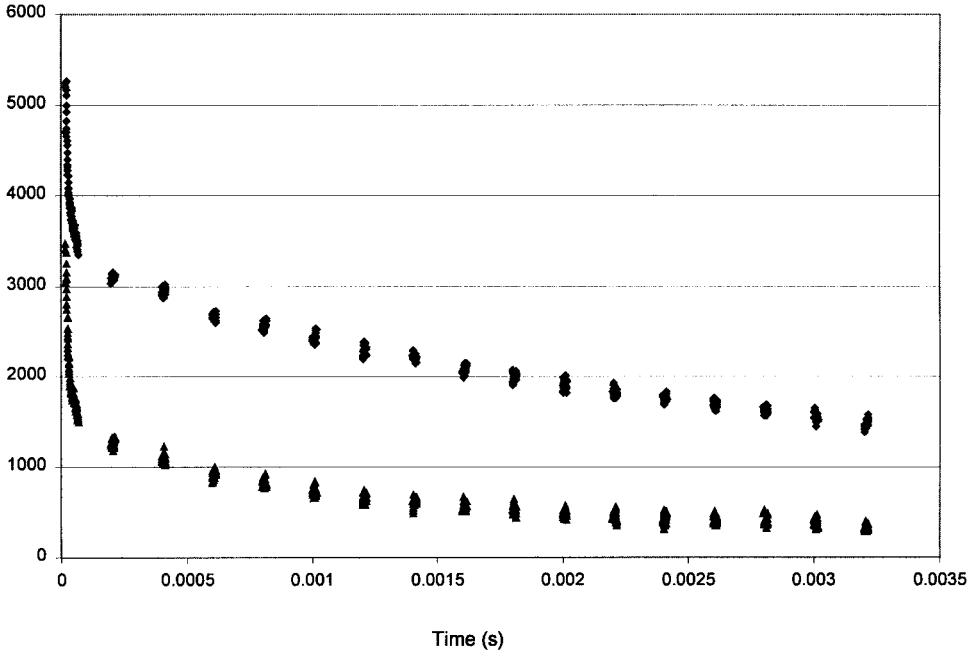

Figure 2 Time-dependent NMR signal amplitude of water in pollen grains at two different water contents (22% and 4.5%, upper and lower curves, respectively) as measured after excitation of the spin system at $t = 0$. The duration of the excitation pulse was 3.7 μm. The initial part of the signal is the so-called free induction decay, FID. After 100 μs a refocusing pulse is applied, resulting in an echo at 200 μs. The refocusing pulse is

depend on the pore size and its distribution, the type of biofilm/biocatalyst (minerals, organic matter, content of paramagnetic ions) and the water content. The relationship between the relaxation times of water and its physical environment has been utilised to characterise the porosity of soils and sediments [20]. For a particular system, T_1 values have been used successfully to estimate the permeability of the solid matrix [18] as well as the wettability [17]. T_2 measurements have also proven to be highly correlated to the surface area and pore-size distribution [24]. T_2 measurements of water in microporous biosystems can, however, be affected by the so-called susceptibility artifacts, resulting from the difference in magnetic permeability of air, water and solid matrix materials, creating local distortions of the magnetic field value, resulting in local magnetic field gradients. Due to these susceptibility artifacts, the observed T_2 values are strongly dependent on the details of the experiment to measure T_2 relaxation, e.g., the interpulse distance or echo time TE [63]. The susceptibility effect can be minimized by the use of low magnetic field strength and short TE values [12]. By doing so, T_2 in addition to T_1 also becomes a very useful parameter to characterise porous biosystems [31].

NMR and transport processes in porous biosystems

Transport processes of water (or other fluids) and of molecules or ions dissolved therein can be measured by NMR in a number of different ways. Here we demonstrate three strategies:

- mapping the (spin) displacement in a well-defined time interval directly based on PFG or displacement imaging
- mapping the effect of contrast agents (paramagnetic molecules/ions) *via* single-parameter spin relaxation time images or *via* spin relaxation time weighted images
- following the amount of spins (water) in time-controlled sequential quantitative spin-density images

Direct transport measurements by use of pulsed magnetic field gradients

Principle: A net unidirectional displacement R of an ensemble of identical spins between two magnetic field gradient pulses of duration δ and of amplitude G, separated in time by Δ, in the direction of that gradient results in a net phase shift *phi;* of the NMR signal:

$$\phi = \gamma \delta G R \tag{2}$$

where γ is the gyromagnetic ratio of the observed spin. If a number of ensembles of spins contribute to the NMR signal the observed signal S is given by:

$$S \sim \int p(r_0) \int P(r_0|r_0+R,\Delta)\ \exp(i\gamma\delta G R)\ d(r_0+R)\ dr_0 \tag{3}$$

where $p(r_0)$ is the probability of finding a spin at r_0 at time zero and $P(r_0|r_0+R_1,\Delta)$ is the conditional probability that a spin originally at r_0 at time zero (the time of the first magnetic field gradient pulse) will be at r_0+R at $t=\Delta$ of the second pulse. The integration is over all starting and end positions. Note from Equation 3 that the signal is complex, consisting of a real (or in-phase) and an imaginary (or out-of-phase) part.

From Equation 3 it is clear that a random distribution of displacements with respect to G does not result in a net phase shifted signal, but in a decrease of the signal amplitude. This will be the case for, e.g., diffusion and dispersive flow perpendicular to the net flow direction. In contrast, net flow will result in a net phase shift.

Diffusion is measured by recording the signal amplitude as a function of gradient strength G. For free, unhindered, diffusion this results in

$$A = A(\mathrm{TE})\ \exp(-Db) \tag{4}$$

with $b=\gamma^2\delta^2G^2\ (\Delta-1/3\delta)$, D is the (self-)diffusion coefficient and $^{\mathrm{A}}(\mathrm{TE})$ is the echo amplitude without gradients (cf. Equation 1). By varying Δ, the displacement can be followed as a function of observation time, allowing one to trace the distance over which the spins can displace. In this way the structure in which the fluid flows or diffuses (pore size and geometry) can be probed *via* observing effects of displacement restrictions by impermeable walls (restricted diffusion). The behaviour of the complex NMR signal amplitude for different types of motion is presented in Table 1.

Flow measurements in porous biosystems by PFG can be done in a number of ways [63], single shot at a fixed G and Δ value, either localised, but nonspatially resolved within this localisation [52], or in combination with imaging [34]. The advantage of this strategy is the short measurement time, allowing a high time resolution. The main disadvantage is that quantification of the measurements in terms of flow velocity requires knowledge of the flow profile, containing its distribution of velocity and direction (cf. Equation 3 and Table 1). To overcome the latter problem one can measure the signal intensity as a function of the gradient amplitude G. It can be shown from Equation 3 that a

Table 1 PFG-SE or PFG-STE amplitude modulation factor for different types of motion

Type of motion	First echo real part	First echo imaginary part	Ref.
diffusion	$\exp(-bD)$	0	[54]
plug flow	$\cos(cv)$	$\sin(cv)$	[15]
laminar flow	$\frac{\sin(cv_o)}{cv_o}$	$\frac{1-\cos(cv_o)}{cv_o}$	[15]
Perfusion			
plug flow[a,b]	$\frac{\sin(\lvert c\rvert v)}{\lvert c\rvert v}$	0	[28]
laminar flow[b]	$\frac{\mathrm{Si}(cv_o)}{cv_o}$	0	[28]
model II[c]	$\exp(-\mathrm{bD}')$	0	[28]

$\mathrm{c}=\gamma\mathrm{G}\delta\Delta$, $\mathrm{b}=(\gamma\delta\mathrm{G})^2(\Delta-1/3\delta)$, $\mathrm{D}'=(\langle 1\rangle\langle \mathrm{v}\rangle)/2$, with $\langle \mathrm{v}\rangle$ the average velocity and $\langle 1\rangle$ the average distance along which spins move with constant velocity [28].

[a]Distribution of equal, straight capillaries, randomly oriented with respect to the gradient.

[b]Capillary flow profile, with v_o as the maximum velocity.

[c]The mean distance travelled by the moving spins during the interval Δ is in this model longer than the mean capillary length, thus the direction of flow changes several times during this period.

Fourier transformation of S as a function of G results in the average propagator $P_s(R, \Delta)$, representing the probability that a spin at any initial position is displaced by R over time Δ. By dividing $P_s(R, \Delta)$ by Δ the flow profile is obtained directly. This type of measurements, referred to as displacement or q-space imaging, has been applied for flow in different porous (bio-)systems and turns out to be very powerful [29,41,44,48–51,53,58–62,65]. It should be noted that this full propagator approach requires relatively strong magnetic field gradients. If such strong gradients are not available these measurements are limited to longer Δ values.

Applications: Following the pioneering work of Stejskal and Tanner [54], PFG NMR can be used for measuring diffusion coefficients in systems ranging from unrestricted bulk diffusion in liquids [5,28] to the much slower motion of, for example, sorbed molecules in zeolites [19] or restricted diffusion in porous media or microorganisms [28]. In systems with a combination of free, unrestricted diffusive water and water confined in microorganisms it is possible to discriminate both in a diffusion-weighted NMR experiment, allowing one to, e.g., assay the bacteria population in porous media and soils [43].

Central to the understanding of diffusion-controlled mass transfer kinetics in porous particles is the effective diffusivity (D_{eff}) of and in the nonflowing ("stagnant") fluid entrained in the intraparticle pore network of the porous biosystem. D_{eff} is defined by Fick's first law:

$$J = -D_{\text{eff}} dC/dx, \tag{5}$$

where J is the flux through the biofilm and C the solute concentration in the liquid phase. D_{eff} is related to the bulk diffusivity in the free solution, D_{aq}, or the transient diffusivity, D_s, by:

$$D_{\text{eff}} = D_{\text{aq}}(\varepsilon_{\text{intra}}/\tau_{\text{intra}}) = D_s \varepsilon_{\text{intra}} \tag{6}$$

with $\varepsilon_{\text{intra}}$ the internal porosity of the particle and τ_{intra} the tortuosity factor [55]. In general, D_{eff} is the transport parameter relating the diffusive flux into and out of the pores to the morphology (geometry and topology) of the pores. D_{eff} includes surface characteristics (e.g., roughness or chemical modification), the pore size and its distribution, pore shape, and pore interconnectivity. The diffusion coefficient measured by NMR correlates to D_s [3]. Diffusion coefficients determined by NMR in both well-defined biofilms and in spontaneously grown aggregates corresponded well to glucose diffusion coefficients determined by microsensors in the same matrices (Table 2). Thus NMR measurements provide an easy way to determine the diffusivity of natural biofilms [3].

The effective (or apparent) diffusivity D_{eff} can be calculated from D_s if the porosity is known. PFG NMR in combination with T_2 imaging has been used for single parameter imaging of the same object: amplitude (A), the relaxation time T_2, and the diffusion coefficient (D_s) [68]. The amplitude image is directly related to the proton density, i.e., the amount of protons per defined volume. By normalising this amplitude on that of pure water, it directly reflects the porosity if only extracellular water in the biofilm contributes to the observed NMR amplitude. This information has recently been used to derive fine-scale D_{eff} images of microbial mats [71]. The apparent water diffusivity obtained in this way by NMR compared well to apparent O_2 diffusivities measured with a diffusivity microsensor [71].

Table 2 Comparison of diffusion coefficients determined by PFG NMR and glucose microsensors (after Bueling *et al* [3])

Porous system	D_{rel} measured by PFG NMR	D_{rel} measured by glucose microsensor
Agar beads		
1.5% w/v	0.96	0.96
3% w/v	0.93	0.92
4% w/v	0.89	0.90
Agar beads (1.5% w/v) supplemented with polystyrene particles		
8% (homogeneous)	0.99	0.91
8% (inhomogeneous)	0.97	0.90
15% (homogeneous)	0.88	0.87
20% (homogeneous)	0.87	0.86
20% (inhomogeneous)	0.84	0.80

Data are expressed as a relative diffusion coefficient (D_{rel}), the ratio of the measured diffusion coefficient in the beads over the diffusion coefficient in free water at the same temperature.

The potential of ^{1}H PFG NMR for flow characterisation, intraparticle diffusivity and mass transfer (exchange) kinetics between the stagnant mobile phase in porous beads and the interparticle void space surrounding these beads has been demonstrated by *Tallarek et al* [58–62]. Figure 3 presents two average propagators $P_s(R, \Delta)$ obtained in these systems at two different labelling times Δ. At short Δ value two separate peaks are observed, one centred on zero displacement ("stagnant" water in the pores of the porous bead) and one related to the flowing water in the interparticle space. The centre position of the second peak reflects the average flow velocity and the width of the (interparticle) dispersion coefficient. These net flow and dispersive flow components could be measured at time scales and displacement distances ranging from the interparticle subpore to several pore dimensions. These rather short displacements cover the distance typical for the correlation length (in the order of the bead diameter, which ranged from 30 to 1300 μm) of these systems. In addition, the width of the stagnant water peak allows the determination of the intraparticle diffusivity whereas the integral of this peak reflects the amount of water still in the particle during time Δ. By measuring this amount of the stagnant water as a function of Δ the mass transfer or exchange kinetics between water in the porous particle and the surrounding flowing water is obtained [61,62]. If the bead diameter and its distribution is known, the combined analyses of the steady state intraparticle pore diffusion data and the associated exchange kinetics can be used to study (the average dimension of) external stagnant fluid layers around these beads [62]. It will be interesting to apply this approach to biofilms or other biosystems.

Average propagator measurements by PFG can also be combined with imaging techniques [5]. The result is an image in which each pixel contains a propagator. In Figure 4 this is demonstrated for an artificial kidney or ultra filtration system, consisting of a large number (~1000) of polysulfon fibres with an inner diameter of 200 μm and porous walls. Figure 4A presents an amplitude image. In Figure 4B typical average propagators are plotted of three pixels in this image. One contains only diffusing water (outside the capillaries), the second only flowing water (inside a capillary) and the third a mix of both (this pixel contains part of a capillary and part of the intercapillary space). Images can now be constructed that present the intensity of the average propagator per pixel at a given displacement, as indicated in the

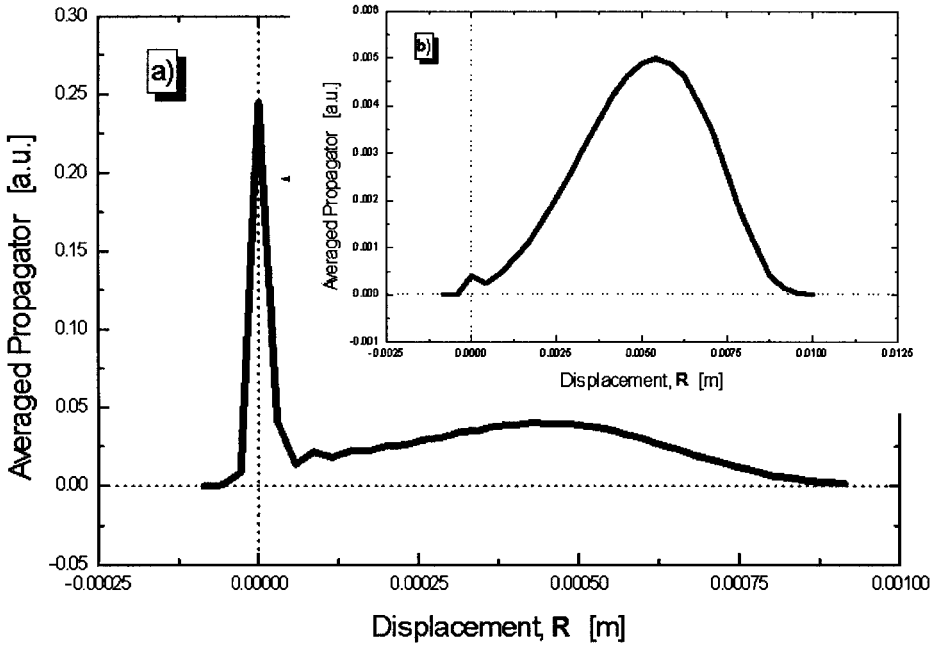

Figure 3 Average propagator curves for axial dispersive flow in a column packed with porous particles of 50 μm diameter (after Tallarek *et al* [62]). (a) $\Delta = 25$ ms. At this time scale there is no complete exchange between water in the porous particles and the flowing water in the interparticle space; (b) $\Delta = 420$ ms. Now the exchange between both water pools is nearly complete.

images. In this way the homogeneity of the flow profile and thus the efficiency of this filtration system can be tested. Comparable approaches can be found in studying the growth of bacterial or cell cultures in these hollow fibre reactor, for the performance of chromatography columns [58] and bead packings [51] and for transport studies in plants [49].

As is evident from the results presented in Figure 4, it is possible that different water pools or proton pools contribute to the signal, both in imaging and in nonimaging mode measurements. A small number of techniques is available to discriminate these water or proton pools. Combined PFG and T_2 relaxation time measurements have been performed that allow for the discrimination of moving protons with different relaxation behaviours, which reflects different (physical) environments within the system [66]. In this way, in sephadex–water systems flowing water outside the sephadex beads and diffusing water in the beads have been discriminated [67]. This method has also been used in imaging mode [68]. Alternatively, PFG NMR measurements can be combined with spectroscopy to discriminate on the basis of chemical shift differences [56,70].

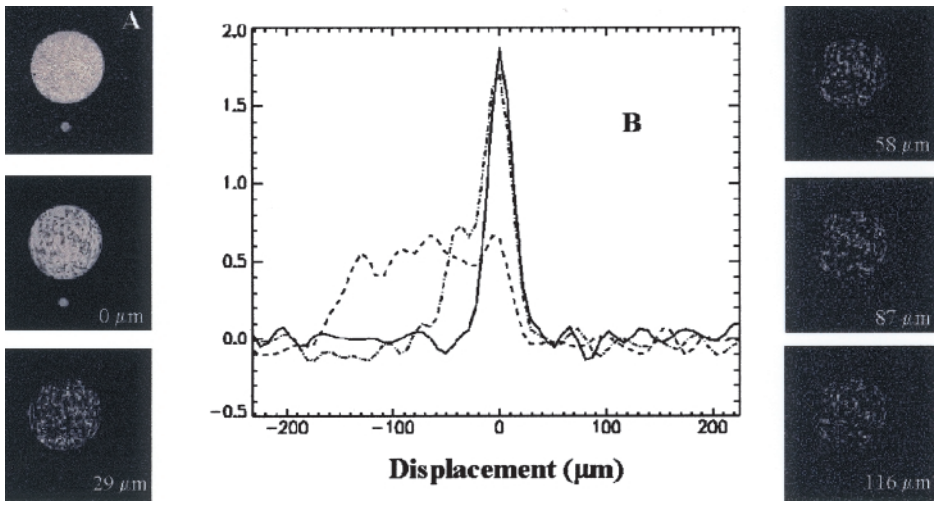

Figure 4 (A) Amplitude image of an ultrafiltration system (artificial kidney) consisting of about 1000 polysulfon fibres (inner diameter 200 μm, permeable walls). The water outside the fibres is nonflowing, whereas in the fibres it flows. (B) Average propagator curves of three pixels of the image presented in (A). The other images present the intensity per pixel at certain displacements, representing the amount of water that was displaced over 0, 29, 58, 87 and 116 μm within Δ (= 21.26 ms). The small dot of water beneath the kidney is a reference tube filled with water. Parameters: field of view 20 mm, slice thickness 3 mm. Courtesy of T Scheenen, D van Dusschoten, PA de Jager and H Van As.

PFG NMR is not restricted to water transport, and has also been applied to study transport of oily emulsions and light oil in porous rocks [35] or sediments/sludges [45], of nonaqueous phase liquid (NAPL) in a simulated pump-and-treat remediation process [14] as well as water, glycerol and very immobile components in *Pseudomonas aeruginosa* biofilms [70].

Time window and resolution: In general, the spatial resolution is at the expense of the signal-to-noise ratio per pixel. To date, a spatial resolution of up to 10 μm can be obtained for ^{1}H of water, thus enabling NMR microscopy of individual plant and mammalian cells [1]. However, for most environmental applications, e.g., biofilms, sludges and soils, a spatial resolution of about 50–100 μm is more realistic. The images in Figure 4 of the hollow fibre reactor have an in plane spatial resolution of 200×200 μm and a thickness of the slice of 2 mm.

For a reliable determination of $P_s(R, \Delta)$, S has to be measured as a function of a minimal 32 different gradient values. It is clear that this takes time. As mentioned before, a two-dimensional SE image consisting of $N \times N$ picture elements requires N acquisitions to be repeated. Combining this with q-space with 64 gradient steps results in $64 \times N$ acquisitions. Doing so is very time consuming (several hours). Alternatively, q-space displacement imaging has been combined with fast turbo spin–echo (TSE) imaging [49], resulting in a N/m times faster sequence compared to a standard $N \times N$ SE image sequence. Here m is the turbo factor, equal to the number of echoes that can be acquired in one scan. Alternatively, an even faster line scan sequence has been presented, in which two slice-selective rf pulses are used to define a line in the object or system to be measured [69]. Within this observation line the normal one-dimensional spatial resolution can be obtained. This results in an N times faster sequence compared to a 2D SE image sequence, but with reduced spatial resolution in one dimension.

In PFG experiments the time window used to observe transport phenomena equals the observation time Δ, which is restricted by the relaxation times [49,52]. At low water contents, these values can become so short that PFG-NMR can be used no longer. Then transport has to be measured by following the water intensity in time-controlled sequential images (see below).

Transport of contrast agents or labelled molecules

Principle: A large number of paramagnetic ions exists, which are not directly observable by NMR, but which shorten the T_1 and/or T_2 of the molecules in contact with them. NMR imaging measurements of dispersion of paramagnetic tracers in heterogeneous media *via* this relaxation dependence have been published [26,40]. The effect of such tracer ions on the relaxation times depends on the nature of the ion and on its (local) concentration. To become visible the paramagnetic tracer has to affect the observed relaxation time:

$$1/T_{\text{obs}} = 1/T_{\text{int}} + 1/T_{\text{tracer}} \qquad (7)$$

where T_{obs} represents either the observed T_1 or T_2, T_{int} the intrinsic relaxation time value of the fluid under observation and T_{tracer} the contribution to the fluid relaxation due to the presence of the tracer molecules. The latter term depends on the nature of the tracer and its (local) concentration.

Image contrast differences have been used to measure transport of these ions [37,38]. Contrast difference can be used for quantification of transport if the water content is constant in time. If not, a unique and real quantitative interpretation of the transport of these ions can only be obtained by quantitative single-parameter T_1 or T_2 images in combination with A_0 images. *Via* quantitative T_1 or T_2 and A_0 images, the presence, concentration and transport behaviour of these ions (*via* time-controlled sequential T_1 or T_2 and A_0 images) can be visualised.

Examples of tracer molecules that can be used for this type of study include: Mn^{2+}, Cu^{2+}, Fe^{2+}, and Gd^{3+}. Moreover, also metals chelated by organic matter, e.g., Mn–EDTA^{2-}, Fe–dextran or Gd–DTPA^{2-} can be traced. These ions and molecules can be manufactured in a variety of sizes, e.g., Fe–dextran particles can range from <0.01 μm to >10 μm. Thus, one can study the behaviour of these chelated organic molecules in a porous biosystem as a function of size, molecular weight, charge and chemical nature.

Applications: Figure 5 gives an example of the penetration of Mn^{2+} into a sediment. At time zero a layer of water doped with $MnCl_2$ is placed on the top of the water-saturated sediment,

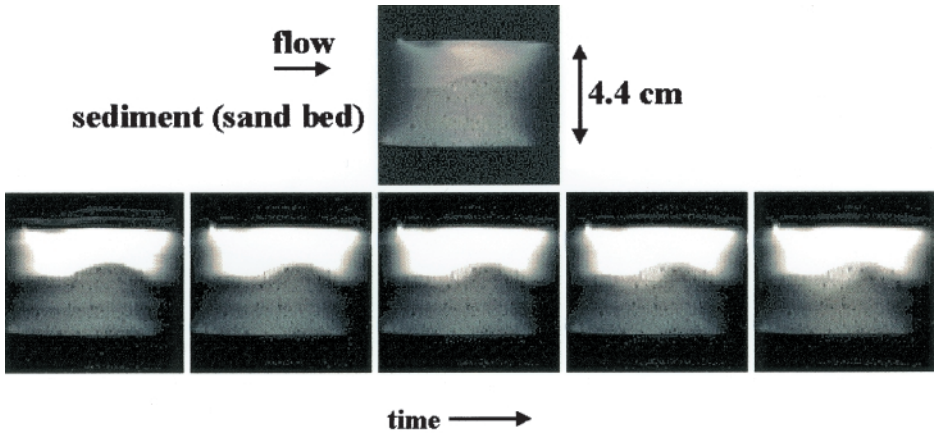

Figure 5 Images demonstrating the determination of sediment flow. Water flowed with constant velocity over a sand bed, with a small hill on top of it (upper image). In the second series of images, taken at well-defined time intervals, $MnCl_2$ is added to the water and the penetration of Mn ions into the sand bed is observed by changes in image contrast due to changes in relaxation times of water in contact with the Mn ions. Sediment flow is obtained in different directions by displaying the intensity profiles at different time steps in the desired direction. Courtesy of D de Beer, H Van As, D van Dusschoten and W Kuhl.

which contains a small hill. By applying TSE imaging and rather short repetition times only protons with short relaxation times appear as bright signals. After some time, Mn^{2+} ions have penetrated into the upper part of the sediment, forced by the flow around the hill, where they shorten the T_2 values of water, resulting in brighter signals. In this way the penetration profile can be followed in time [10].

Time window and resolution: The time resolution for this type of measurement is given by the time to acquire the data for one image, which typically range for water from some seconds to several minutes. The time window over which transport can be followed is hardly limited, because the sample under study can be measured repeatedly, over a period covering weeks or months.

Transport measurements based on time-controlled sequential spin-density images

Principle: For reliable transport studies it is necessary to obtain quantitative spin-density images representing $A_0(r)$, which are not affected by the other parameters like the relaxation times. Quantitative spin-density images can be obtained by use of multiecho imaging [11,12], followed by an extrapolation of the amplitude images to TE=0 (cf. Equation 1). In this way the amplitude images are only influenced by the characteristics of the sensitivity profile of the NMR rf coil [13].

Applications: Flow and transport phenomena can now be studied by following the spin density in time by repeated imaging, resulting in $A_0(r,t)$. This type of transport measurement is only useful in nonstationary density situations, e.g., relatively slow re- and dehydration and penetration processes. Figure 6 illustrates this approach to follow solid-substrate fermentation processes of a fungus grown on a wheat dough [36]. The fungus, which developed on top of the dough, clearly takes up water from the dough as reflected by the (small) decrease in A_o and increase in $1/T_2$ and $1/T_1$. At the same time the fungus excretes α-amylase, resulting in formation of glucose in the dough. In this system part of the water is relaxing too fast to be observed (cf. Figure 2) and the amplitude image therefore only represents the more mobile water fraction. Both $1/T_2$ and $1/T_1$ turned out to be dependent on both water and glucose content of the wheat dough, but in a different way. By proper calibration, the combination of these parameters allowed the authors to calculate the water and glucose profiles in this system as a function of time, thus enabling the modelling of this fermentation process [36].

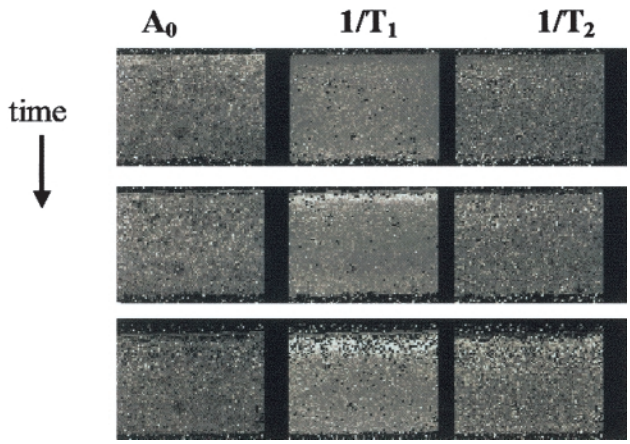

Figure 6 Amplitude (A_0), $1/T_1$ and $1/T_2$ images of a wheat dough system. On top of it is a membrane. At $t=0$ a small amount of mycelium suspension was added on this membrane. A fungus developed by taking up water and glucose from the dough. The fermentation of the dough and development of the fungus are followed in time. Courtesy of FJ Nagel, A Rinzema and H Van As.

Time window and resolution: The limitations and the time window of this method is comparable to that mentioned in the section Transport of contrast agents and labelled molecules. The spatial resolution that can be reached strongly depends on the type of nucleus (NMR sensitivity) and the (local) concentration of the molecule to be imaged [5].

Further developments and perspectives

Bioreactor analysis

MRI of water can be used to generate high resolution images of the internal anatomy, at a theoretical spatial resolution that is less at a low magnetic field strength than at higher fields (typically in the order of $150\times150\times1500$ μm at a magnetic field strength of 0.47 T and $20\times20\times200$ μm at 9.4 T, for a small coil and a total acquisition time of about 4 min). This difference in spatial resolution is due to the higher signal-to-noise ratio (S/N) at high magnetic fields. Our experience is that, because of susceptibility artifacts, which increase with B_0^2, it can be advantageous to work at low field, thereby sacrificing spatial resolution for geometric and functional resolution [11].

NMR procedures, used in combination with imaging and localised spectroscopy techniques, were shown to unravel the flow and transport processes in porous biosystems and enable the monitoring of growth and distribution of cells within a reactor system. When coupling these noninvasive ^{1}H NMR measurements to ^{31}P or ^{23}Na NMR, this type of NMR also allows one to investigate metabolic heterogeneity within a reactor and can assist in future design of bioreactor systems.

Another promising evolution is the development of portable magnets, allowing on-site measurements of single NMR parameters A_0, T_1, T_2 [4] or even flow [64]. Thus, it has become possible to measure directly subsurface geological formations *in situ* by dedicated NMR instruments using T_2 information [21]. One could also consider installing these devices at bioreactors, continuously providing information on transport processes occurring in the cell suspension or sludge or on the water content during solid state fermentation.

A number of parameters that play a role in an MRI experiment are temperature dependent. MR temperature imaging methods, based on the temperature dependence of the molecular diffusion D [19], the spin–spin relaxation time T_1 [72], and the resonance frequency of water protons [42] have been presented. At present this NMR application is used in medicine to monitor temperature changes in real time during tissue heating (hyperthermia, laser surgery, focused ultrasounds) or cooling (cryotherapy). In the context of porous biosystems, temperature mapping can assist in the design of heat-pulsed or temperature-phased bioreactors.

Combination with other NMR techniques

NMR studies are not restricted to water transport or water flow, but can also be used for other proton or other nuclei (e.g., ^{2}H or ^{19}F) bearing molecules [33,46], e.g., by discrimination on the basis of chemical shift differences. Vogt *et al* [70] applied this method to a *P. aeruginosa* biofilm.

Solid-state NMR spectroscopy is nowadays a well-established technique used for structure elucidation and to describe the pore architecture, catalytic behaviour and mobility properties (like diffusion) of zeolites [57]. Important framework elements such as ^{27}Al, ^{29}Si and ^{31}P can be studied directly by NMR. Also, ^{129}Xe is a suitable and sensitive isotope for probing the pore architecture of zeolitic materials. Much of the work performed with zeolites can be applied to other porous filtration or absorption/adsorption materials, e.g., ion-exchange resins, peat and activated carbon. It may be expected that this research will contribute to a better design of bioreactors.

Acknowledgements

We thank Dr U. Tallarek and Ir T. Scheenen for fruitful discussions during the preparation of this manuscript, and for making available Figures 3 and 4, respectively. Figures 5 and 6 were prepared courtesy of Dr D. de Beer and Ir F.-J. Nagel, respectively. This work was in part supported by an EU Human Capital and Mobility grant ERBCHGECT 940061 (access to large-scale facility Wageningen NMR Centre) and a European Community Marie Curie fellowship (ERBFMBICT950250).

References

1 Aiken NR, EW Hsu and SJ Blackband. 1995. A review of NMR microimaging studies of single cells. *J Magn Reson Anal* 1: 41–48.
2 Bear J and MY Corapcioglu. 1984. Fundamentals of Transport Phenomena in Porous Media. Martinus Nijhoff Publ., Dordrecht.
3 Beuling EE, D van Dusschoten, P Lens, JC van den Heuvel, H van As and SPP Ottengraf. 1998. Characterization of the diffusive properties of biofilms using pulsed field gradient nuclear magnetic resonance. *Biotech Bioeng* 60: 283–291.
4 Blümich B, P Blümler, G Eidmann, A Guthausen, R Haken, U Schmitz, K Saito and G Zimmer. 1998. The NMR-MOUSE: construction, excitation and applications. *Magn Reson Imaging* 16: 479–484.
5 Callaghan PT. 1991. Principles of Nuclear Magnetic Resonance Microscopy. Clarendon Press, Oxford.
6 Caprihan A and E Fukushima. 1990. Flow measurements by NMR. *Phys Rep* 198: 195–235.
7 Chaouki J, F Larachi and MP Dudukovic. 1997. Noninvasive tomographic and velocimetric monitoring of multiphase flows. *Ind Eng Chem Res* 36: 4476–4503.
8 Chen S, X Yao, J Qiao and AT Watson. 1995. Characterisation of fracture permeable porous media using relaxation-weighted imaging techniques. *Magn Reson Imaging* 13: 599–606.
9 de Beer D, P Stoodley and Z Lewandowski. 1997. Measurement of local diffusion coefficients in biofilms by microinjection and confocal microscopy. *Biotech Bioeng* 53: 151–158.
10 de Beer D, M Kuhl, D van Dusschoten and H Van As. 2000. A comparison between micro-sensor and NMR transport measurements in sediments. Manuscript in preparation.
11 Edzes HT, D van Dusschoten and H Van As. 1998. Quantitative T_2 imaging in plant tissues by means of multi-echo MRI microscopy. *Magn Reson Imaging* 16: 185–196.
12 Donker HCW, H Van As, HT Edzes and AHW Jans. 1996. NMR imaging of white button mushroom (*Agaricus bisporus*) at various magnetic fields. *Magn Reson Imaging* 14: 1205–1215.
13 Donker HCW, H Van As, HJ Snijder and HT Edzes. 1997. Quantitative 1H-NMR imaging of water in white button mushrooms (*Agaricus bisporus*). *Magn Reson Imaging* 15: 113–121.
14 Gladden LF. 1996. Structure–transport relationships in porous media. *Magn Reson Imaging* 14: 719–726.
15 Hemminga MA and PA de Jager. 1980. The study of flow by pulsed nuclear magnetic resonance: II. Measurement of flow velocities using a repetitive pulse method. *J Magn Reson* 37: 1–16.
16 Heys AWJ and CP Lowe. 1995. Numerical evaluation of the permeability and the Kozeny constant for two types of porous media. *Phys Rev E* 51: 4346–4352.
17 Howard JJ. 1994. Wettability and fluid saturations determined from NMR T_1 distributions. *Magn Reson Imaging* 12: 197–200.
18 Issa B and P Mansfield. 1994. Permeability estimation from T_1 mapping. *Magn Reson Imaging* 12: 213–214.
19 Kärger J and DM Ruthven. 1992. Diffusion in Zeolites and Other Microporous Solids. Wiley, New York.
20 Kenyon WE. 1992. Nuclear magnetic resonance as a petrophysical measurement. *Nucl Geophys* 6: 153–171.
21 Kleinberg RL, A Sezginer, DD Griffin and M Fukuhara. 1992. Novel NMR apparatus for investigating an external sample. *J Magn Reson* 97: 466–485.
22 Kleinberg RL. 1994. Pore size distributions, pore coupling and transverse relaxation spectra of porous rocks. *Magn Reson Imaging* 12: 271–274.
23 Kleinberg RL, A Sezginer, DD Griffin and M Fukuhara. 1992. Novel NMR apparatus for investigating an external sample. *J Magn Reson* 97: 466–485.
24 Kleinberg RL, WE Kenyon and PP Mitra. 1994. Mechanism of NMR relaxation of fluids in rocks. *J Magn Reson A* 108: 206–214.
25 Kühl M and NP Revsbech. 2000. Microsensors for the study of interfacial biogeochemical processes. In: Boudreau B and BB Jørgensen (Eds), The Benthic Boundary Layer: Transport Processes and Biogeochemistry. Oxford Press, in press.
26 Kutchovsky YE, V Alvarado, HT Davis and LE Scriven. 1996. Dispersion of paramagnetic tracers in bead packs by T_1 mapping: experiments and simulations. *Magn Reson Imaging* 14: 833–840.
27 La Heij EJ, PJAM Kerkhof, K Kopinga and L Pel. 1996. Determining porosity profiles during filtration and expression of sewage sludge by NMR imaging. *AICHE J* 42: 953–959.
28 Le Bihan D. 1991. Molecular diffusion nuclear magnetic resonance imaging. *Magn Res Q* 7: 1–30.
29 Lebon L, L Oger, J Leblond, JP Hulin, NS Martys and LM Schwartz. 1996. Pulsed gradient NMR measurements and numerical simulation of flow velocity distribution in sphere packings. *Phys Fluids* 8: 293–301.
30 Lens PNL and MA Hemminga. 1998. Nuclear magnetic resonance in environmental engineering: principles and applications. *Biodegradation* 9: 393–409.
31 Lens P, F Vergeldt, G Lettinga and H van As. 1999. ^{1}H-NMR study of the diffusional properties of methanogenic aggregates. *Water Sci Technol* 39 (7): 187–194.
32 Lewandowski Z, SA Altobelli and E Fukushima. 1993. NMR and microelectrode studies of hydrodynamics and kinetics in biofilms. *Biotechnol Prog* 9: 40–45.
33 Link J and J Seelig. 1990. Comparison of deurerium NMR imaging methods and applications to plants. *J Magn Reson* 89: 310–330.
34 Mansfield P and B Issa. 1994. Studies of fluid transport in porous rocks by echo-planar MRI. *Magn Reson Imaging* 12: 275–278.
35 Mardon D, MG Prammer and GR Coates. 1996. Characterization of light hydrocarbon reservoirs by gradient-NMR well logging. *Magn Reson Imaging* 14: 769–777.
36 Nagel FJ, A Rinzema and H Van As. 2000. MRI applied to study the water balance during solid substrate fermentation in a fungus/wheat dough system. *Biotech Bioeng* (submitted for publication).
37 Nestle N and R Kimmich. 1996. Heavy metal uptake of alginate gels studied by NMR microscopy. *Colloids Surf, A* 115: 141–147.
38 Nestle N and R Kimmich. 1996. NMR microscopy of heavy metal absorption in calcium. *Appl Biochem Biotechnol* 56: 9–17.
39 Okabe S, T Yasuda and Y Watanabe. 1997. Uptake and release of inert fluorescent particles by mixed population biofilms. *Biotechnol Bioeng* 53: 459–469.
40 Oswald S, W Kinzelbach, A Greiner and G Brix. 1997. Observation of flow and transport processes in artificial porous media *via* magnetic resonance imaging in three dimensions. *Geoderma* 80: 417–429.

41 Packer KJ and JJ Tessier. 1996. The characterization of fluid transport in a porous solid by pulsed gradient stimulated echo NMR. *Mol Phys* 87: 267–272.
42 Peters RD, RS Hinks and RM Henkelman. 1999. Heat-source orientation and geometry dependence in proton-resonance frequency shift magnetic resonance themometry. *Magn Reson Med* 41: 909–918.
43 Potter K, RL Kleinberg, FJ Brockman and EW McFarland. 1996. Assay for bacteria in porous media by diffusion-weighted NMR. *J Magn Reson, Ser B* 113: 9–15.
44 Rajanayagam V, S Yao and J Pope. 1995. Quantitative magnetic resonance flow and diffusion imaging in porous media. *Magn Reson Imaging* 13: 729–738.
45 Reeves AD and JA Chudek. 2000. Nuclear magnetic resonance (NMR) studies of oil residues in environmental substrates. *J Ind Microbiol*, this issue.
46 Sarkar SN, JJ Dechter and RA Komoroski. 1993. Multinuclear NMR imaging of fluid phases in berea sandstone. *J Magn Reson Series A* 102: 314–317.
47 Sato H, S Eto and H Suzuki. 1980. Studies on the state of water in sludges by high-resolution NMR. *Nippon Kagaku Kaishi* 3: 354–358.
48 Schaafsma TJ, H Van As, WD Palstra, JEM Snaar and PA de Jager. 1992. Quantitative measurement and imaging of transport processes in plants and porous media by ^{1}H NMR. *Magn Reson Imaging* 10: 827–836.
49 Scheenen TWJ, D van Dusschoten, PA de Jager and H Van As. 2000. Microscopic displacement imaging with pulsed field gradient turbo spin–echo NMR. *J Magn Reson* 142: 207–215.
50 Seymour JD and PT Callaghan. 1996. Flow-diffraction structural characterization and measurment of hydrodynamic dispersion in porous media by PGSE NMR. *J Magn Reson, Ser A* 122: 90–93.
51 Seymour JD and PT Callaghan. 1997. Generalized approach to NMR analysis of flow and dispersion in porous media. *AIChE J* 43: 2096–2111.
52 Snaar JEM and H Van As. 1990. Discrimination of different types of motion by modified stimulated-echo NMR. *J Magn Reson* 87: 132–140.
53 Stapf S, KJ Packer, S Bekri and Adler. 2000. Two-dimensional nuclear magnetic resonance measurements and numerical simulations of fluid transport in porous rocks. *Phys Fluids* 12: 566–580.
54 Stejskal EO and JE Tanner. 1965. Spin diffusion measurements: spin echoes in the presence of a time dependent field gradient. *J Chem Phys* 42: 288–293.
55 Stewart PS. 1998. A review of experimental measurements of effective diffusive permeabilities and effective diffusion coefficients in biofilms. *Biotech Bioeng* 59: 261–272.
56 Stilbs P. 1987. Fourier transform pulsed-gradient spin–echo studies of molecular diffusion. *Prog Nucl Magn Reson Spectrosc* 19: 1–45.
57 Stöcker M. 1996. Characterization of zeolitic materials by solid-state NMR — state of the art. In: Chon H, SI Woo and S-E Park (Eds), Vol 102. Elsevier, Amsterdam, pp. 141–189.
58 Tallarek U, K Albert, E Bayer and G Guiochon. 1996. Measurement of transverse and axial apparent dispersion coefficients in packed beds. *AIChE J* 42: 3041–3054.
59 Tallarek U, E Bayer, D van Dusschoten, T Scheenen, H Van As, G Guiochon and UD Neue. 1998. Dynamic NMR microscopy of chromatographic columns. *AIChE J* 44: 1962–1975.
60 Tallarek U, D van Dusschoten, H Van As, E Bayer and G Guiochon. 1998. Study of transport phenomena in chromatographic columns by pulsed field gradient NMR. *J Phys Chem B* 102: 3486–3497.
61 Tallarek U, D van Dusschoten, H Van As, G Guiochon and E Bayer. 1998. Direct observation of fluid mass transfer resistance in porous media by NMR spectroscopy. *Angew Chem, Int Ed* 37: 1882–1885.
62 Tallarek U, FJ Vergeldt and H Van As. 1999. Stagnant mobile phase mass transfer in chromatographic media: intraparticle diffusion and exchange kinetics. *J Phys Chem B* 103: 7654–7664.
63 Van As H and D van Dusschoten. 1997. NMR methods for imaging of transport processes in microporous systems. *Geoderma* 80: 389–403.
64 Van As H, JEA Reinders, PA de Jager, PACM van de Sanden and TJ Schaafsma. 1994. *In situ* plant water balance studies using a portable NMR spectrometer. *J Exp Bot* 45: 61–67.
65 Van As H, W Palstra, U Tallarek and D van Dusschoten. 1998. Flow and transport studies in (non)consolidated porous (bio)systems consisting of solid or porous beads by PFG NMR. *Magn Reson Imaging* 16: 569–573.
66 van Dusschoten D, PA de Jager and H Van As. 1995. Extracting diffusion constants from echo-time-dependent PFG NMR data using relaxation-time information. *J Magn Reson, Ser A* 116: 22–28.
67 van Dusschoten D. 1996. Probing water motion in heterogeneous systems. A multi-parameter NMR approach. PhD thesis, Wageningen Agricultural University.
68 van Dusschoten D, CTW Moonen, PA de Jager and H Van As. 1996. Unravelling diffusion constants in biological tissue by combining CPMG imaging and pulsed field gradient NMR. *Magn Reson Med* 36: 907–913.
69 van Dusschoten D, J van Noort and H Van As. 1997. Displacement imaging in porous media using the linescan NMR technique. *Geoderma* 80: 405–416.
70 Vogt M, H-C Flemming and WS Veeman. 2000. Diffusion in *Pseudomonas aeruginosa* biofilms: a pulsed field gradient NMR study. *J Biotechnol* 77: 137–146.
71 Wieland A, D de Beer, LR Damgaard, M Kuhl, D van Dusschoten and H Van As. Fine-scale measurements of diffusivity in a microbial mat with NMR imaging. *Limnol Oceanogr* (in press).
72 Young IR. 1994. Modeling and observation of temperature changes *in vivo* using MRI. *Magn Reson Med* 32: 358–369.